# Investigations of models and experimental studies of a stationary regime for a laser with a saturable absorber

B. Zambon, F. De Tomasi, D. Hennequin,* and E. Arimondo
*Dipartimento di Fisica, Università delgi Studi di Pisa, piazza Torricelli 2, 56100 Pisa, Italy*
(Received 18 November 1988)

The laser with saturable absorber (LSA) with level structures in amplifier and absorber media has been modeled in a rate-equation approach introducing memory functions. This approach has been applied to vibrational structures in a $CO_2$ medium and rotovibrational structures in molecular absorbers. Experimental results for the LSA regimes with inhomogeneously and homogeneously broadened absorbers are presented. The theoretical results for the laser threshold and the Hopf bifurcation are derived by the model through a fitting of the laser-absorber coupling parameters.

## I. INTRODUCTION

The laser with a saturable absorber (LSA) is currently the subject of many studies both from the point of view of dynamical system theory and from the point of view of competing matter-field interaction between the absorber and amplifier media. In the first case the possibility of modeling the LSA with a small number of equations (the laser mode representing only one degree of freedom) makes available a prototype of a simple nonlinear dynamical system in which chaotic behavior can eventually be found. In the latter case, the study of the stationary and dynamical regimes of the system displays information about the molecular microscopic phenomena at the basis of the absorber and amplifier responses to an electromagnetic (em) field.[1]

The equations ruling the behavior of the LSA are derived from the evolution of the density matrix of the atom system, whose level structure could present some degree of complexity, under the simultaneous influence of the em field and the collisions with surrounding atoms or molecules. Many LSA studies for both the static and dynamic regimes have been devoted to the case of a two-level molecular system. The reason behind that choice was, beyond the need to simplify as much as possible the analysis of this system, the belief that most of the interesting physical behavior would arise mainly from the nonlinear nature of the interaction between two damped oscillators (or more than two in the case of inhomogeneously broadened transition), i.e., the cavity mode and the molecular system. In spite of this simplification the dynamical behavior of the resulting set of equations has been shown to provide a very interesting and rich behavior giving rise to many optical instabilities. Among them the self-oscillating regime of passive $Q$ switching (PQS) has received great attention with the aim of producing very intense and short laser pulses.

However, as the first experiments on the LSA with $CO_2$ were being carried out, the difficulty of matching the experimental results with the results given by the models became apparent.[2-4] This in part was attributed to the effective optical complexities of a real system not taken into account by a model based on a plane-wave approximation for the field inside the cavity. At the same time new kinds of pulse shapes were observed in correspondence with the self-oscillating PQS regime which could not be interpreted, for a reasonable set of parameter values, by the simplified two-level models. Those pulses characterized by a high-frequency oscillatory tail were reproduced by Tachikawa *et al.* by using a rate equations model in which an important contribution in the relaxation mechanism of the active medium ($CO_2$) was taken into account.[5] A previous effort to consider in some detail the structure of the relaxation mechanism occurring in molecular species was made by Arimondo *et al.*[2] by introducing the complexities of the rotovibrational manifolds in the analysis of the LSA. However, a simplifying assumption on the relaxation rates of the lower level of the amplifier medium prevented them from reproducing the characteristic pulse shapes with oscillating tail. On the contrary, in the Tachikawa *et al.* model the description of the absorber, lacking of any rotovibrational structure, convinced us that a better modeling should be introduced for a more careful comparison between experimental and theoretical results. It appeared to us, through the experimental analysis, that a proper description of the collisional mechanisms was a first and necessary step to improve the fit of LSA experimental data with theoretical ones and, from the theoretical point of view, produce reliable models. In the past a systematic study of laser modeling was already undertaken in conjunction with the development of $CO_2$ laser sources and very sophisticated models of the active medium were developed. Among them the models characterized by a thermodynamic approach to the problem of intraband energy exchanges have been proved to be quite effective in interpreting the stationary laser operating conditions.[6] In these models each vibrational band is characterized by a given temperature and energy balance equations between various vibrational modes are set up. However, even if these descriptions of laser operation have some common roots with the rate-equations approach, both stemming from a philosophy based on coarse-graining procedures, they could hardly describe a dynamical regime of the laser sys-

 ©1989 The American Physical Society

tem where sharp pulses perturb the medium to such an extent that a proper definition of band temperature might not be possible. In the case of a model based on the rate equations we can easily treat the interaction of a given energy level with the heat bath by the introduction of a phenomenological damping rate of its population. In this respect, some recent experiments in which the population dynamics was directly monitored by a tunable diode laser offer the possibility of modeling the $CO_2$ discharge behavior by small number of rate equations through a proper selection of the predominant relaxation mechanisms.[7] As regards the absorption process, the complexity in the absorption spectra of typical molecular gases used in the PQS experiments, combined with the peculiar working conditions for the LSA setups (very low pressure in the absorbing cell), further complicates the theoretical analysis. However, at the present it seems that a more crude approach to the absorber's modeling should be tried before a more complex theoretical investigation is put at work. On the other hand, the improvement of the amplifier analysis in the above quoted papers induces us to suppose that modeling the LSA system with a reduced number of equations remains valuable from the point of view of numerical agreement with experimental measurements.

In this paper we present an improvement on the LSA modeling in which the relaxation mechanisms of the absorber and amplifier media are considered in some detail. We will show how the stationary solutions and the state diagram for the LSA system are interpreted with this new model by performing a comparison with experimental findings on a $CO_2$ laser with $SF_6$ saturable absorber. Experimental results concerning other absorbing gases will be presented but not completely analyzed within the proposed model. The application of the model is completed in a successive paper where the LSA pulsed, oscillatory, and chaotic regimes are analyzed.[8]

The LSA experiments are characterized by additional features that, if included in the theoretical model, add a very large complexity. Most experimental observations of bistability and instability in the LSA are performed with low-pressure absorbers, thus in a regime of inhomogeneously broadened absorption line. The theory of Salomaa and Stenholm,[9(a)] later applied to experimental observations on He-Ne laser with an intracavity absorber,[9(b)] was an early analysis of LSA steady state, bistability, and instability in the presence of saturation of a single velocity class inside the Doppler profile. We have not taken into account in this paper the inhomogeneously broadened transition and we have treated the absorber as an homogeneous one. In fact an important experimental result of this paper is that, quite surprisingly, the ranges of bistable and unstable operation are very similar for homogeneous and inhomogeneous broadened absorption lines. This leads us to believe that the kind of modeling adopted, either homogeneous or inhomogeneous, could not, in some LSA operating conditions, constitute an essential feature of the model. Thus we have made use of a model with a homogeneously broadened transition, as in the presence of an efficient velocity diffusion relaxation mechanism. Most LSA theoretical investigations have been restricted to the fully tuned case, in which the resonant frequencies of the amplifier and absorber media are equal and match the cavity tuning. These restrictions have been lifted in a recent theoretical analysis,[10] where the frequency detunings were included in the LSA analysis by increasing the number of equations, whence the complexity of the numerical analysis. In the present modeling we have eliminated adiabatically the polarizations and considered the laser frequency as an external parameter, therefore obtaining rate equations with absorption and amplifier parameters depending on the frequency detunings.

Section II presents the theoretical modeling. The model that we will adopt in this investigation of the LSA will be essentially one based on the rate-equation approximation. However, that approach will be briefly reviewed, starting from the more basic equations and arriving at the final set of equations, with the purpose of showing some of the major assumptions inherent in our model. We will include a general relaxation mechanism in the form of a memory function, and in particular we will discuss the case of rotovibrational relaxation mechanisms as applied to the LSA analysis. Section III specifies the relaxation mechanisms of the $CO_2$ amplifier medium and of the absorber. Section IV presents the experimental setup and the LSA parameters relative to the experiment. The experimental results for the LSA response are reported in Sec. V and are compared to our modeling in Sec. VI. Some mathematical details are reserved to the Appendixes.

## II. THEORETICAL MODELING

The theory of interaction of a monochromatic radiation field with a molecular or atomic system under the assumption that it can be represented by a two-level quantum system has been extensively discussed by many authors.[11] The basic equations stemming naturally from this assumption are known as the optical Bloch equations or sometimes as the Fermi damped-oscillator equations. The usual approach followed in the solution of these equations consists of separating the slowly varying part of a given variable from the very fast one which varies at the frequency of the driving field. Thus for the laser electric field and for the average value of the polarization operator of an ensemble of $N$ atoms inside the unitary volume, $E$ and $P$, respectively, the slowly varying components are isolated from the fast ones varying at the laser frequency $\omega$. In the case of a system with more than two levels in which only two of them are resonant with the radiation we will suppose that owing to the frequency mismatch the off-diagonal elements of the density matrix are significantly different from zero only for the radiation resonant states. It is shown in Appendix A that under these conditions the effect of all the remaining levels can be represented by a memory function $K(t)$ for the variable difference of population between the resonant levels, which are supposed to have energy separation $\hbar\omega_0$. Neglecting higher-order derivatives of $P$, as well as fast oscillating terms, the modified equations then read

$$\dot{P} = -[\gamma_\perp - i(\omega - \omega_0)]P + i(\mu^2/\hbar)ED \ , \tag{1a}$$

$$\dot{D}=\frac{-i(P^*E-E^*P)}{2\hbar}-\int_0^\infty K(t')[D(t-t')-D^0]dt' \ . \tag{1b}$$

Here $D$ is upper-state population minus lower-state population for $N$ atoms inside the unitary volume. $D^0$ gives the equilibrium value of $D$ (in the absence of the radiation field) determined either from thermal mechanisms or by the presence of an external pumping. $\gamma_\perp$ is the transverse relaxation rate and $\mu$ is the dipole moment matrix element between radiation resonant lower and upper states.

For the particular case of $CO_2$ lasers Eq. (1a) can be transformed into the following one by an adiabatic elimination of the polarization in the consequence of the high value of $\gamma_\perp$ as compared to the rate of change of the other variables:[12]

$$P=-D(\eta'+i\eta'')E \tag{2a}$$

where the $\eta'$ in-phase and $\eta''$ out-phase coupling coefficients are given by

$$\eta'=\frac{\mu^2}{\hbar\gamma_\perp}\frac{-\Delta}{1+\Delta^2}, \quad \eta''=\frac{\mu^2}{\hbar\gamma_\perp}\frac{1}{1+\Delta^2} \ , \tag{2b}$$

and the normalized detuning is given by

$$\Delta=\frac{\omega-\omega_0}{\gamma_\perp} \ . \tag{2c}$$

Here a minus sign has been introduced in Eq. (2a) to take care of the convention adopted for the population difference in the amplifier medium. In a linear cavity with standing-wave radiation, forward and backward waves propagate with slowing varying electric field amplitudes $E_F$ and $E_B$ given by

$$\frac{\partial E_F}{\partial z}+\frac{1}{c}\frac{\partial E_F}{\partial t}=2\pi i\frac{\omega}{c}P_F \ , \tag{3a}$$

$$-\frac{\partial E_B}{\partial z}+\frac{1}{c}\frac{\partial E_B}{\partial t}=2\pi i\frac{\omega}{c}P_B \ , \tag{3b}$$

where $P_F$ and $P_B$ are the slowly varying amplitudes of the forward and backward polarization components generating the field inside the cavity. Since the traveling time of the photon in the cavity is small as compared to the dynamical time scale, we can assume that the transverse and longitudinal profiles of the two fields for the forward and backward waves are not modified in changing from a static to a dynamic regime. Furthermore, for a perfectly reflecting mirror at one end of the laser cavity we must have $E_F=-E_B=E$. This means that the field in the cavity can be represented by one variable only, the field mode amplitude $E$. In turn the population difference $D$ is determined through Eq. (1b) by the square of the total field impinging on the atom. This term can be replaced by $|E_F|^2+|E_B|^2$ if standing-wave effects are neglected and successively transformed into $2|E|^2$ in the limit of the uniform-field approximation.[1] As a result of the above considerations the equations for the evolution of the laser variables can be put into the following form:

$$\dot{E}=-2\pi i\omega(\eta'+i\eta'')DE-kE \ , \tag{4a}$$

$$\dot{D}=-\eta''2|E|^2D/\hbar-\int_0^\infty K(t')[D(t-t')-D^0]dt' \ , \tag{4b}$$

where the last term in Eq. (4a) represents the losses through the mirrors. In a non-plane-wave configuration the constant $k$ will be modified by the addition of a phenomenological term taking into account the diffraction losses. By introducing as a new variable the intracavity intensity $I=c|E|^2/8\pi$ of either the forward or backward wave we can write for a medium uniformly distributed in the cavity and completely filling it:

$$\dot{I}=4\pi\omega\eta''DI-2kI \ , \tag{5a}$$

$$\dot{D}=-16\pi\eta''DI/(\hbar c)-\int_0^\infty K(t')[D(t-t')-D^0]dt' \ . \tag{5b}$$

In the case in which also the absorber is present in the cavity, by neglecting all the internal reflections of the field in passing through regions of different media we can write

$$\dot{I}=4\pi\omega\eta''\frac{L_g}{L}DI-4\pi\omega\overline{\eta''}\frac{L_a}{L}\overline{D}I-2kI \ , \tag{6a}$$

$$\dot{D}=-16\pi\eta''DI/(\hbar c)-\int_0^\infty K(t')[D(t-t')-D^0]dt' \ , \tag{6b}$$

$$\dot{\overline{D}}=-16\pi\overline{\eta''}\overline{D}I/(\hbar c)-\int_0^\infty \overline{K}(t')[\overline{D}(t-t')-\overline{D^0}]dt' \ . \tag{6c}$$

Here all the barred quantities refer to the absorber and have the same meanings as for the amplifier, except that the absorber population variable $\overline{D}$ is defined as the difference between lower and upper states. Then to describe inversion of population in the amplifier and the usual population difference in the absorber we have $D^0>0$ and $\overline{D^0}>0$. $L_g$ and $L_a$ are the lengths of the gain and absorber cells and $L$ is the cavity length. A basic assumption in this set of equations is that both absorber and amplifier have homogeneously broadened lines.

From the stationary solution of Eqs. (6), making use of the time independence of $D$ and $\overline{D}$ in the integrals, it follows that the standard relation for the stationary LSA intensity $I$ of the forward or backward wave is given by

$$I\left(\frac{A}{1+2I/I_{sg}}-\frac{\overline{A}}{1+2I/I_{sa}}-1\right)=0 \ , \tag{7}$$

where the following quantities have been defined:

$$I_{sg}=\frac{c}{8\pi}\frac{\hbar}{\eta''}\mathcal{K}^*, \quad I_{sa}=\frac{c}{8\pi}\frac{\hbar}{\overline{\eta''}}\overline{\mathcal{K}}^* \ , \tag{8a}$$

$$\mathcal{K}^*=\int_0^\infty K(t')dt', \quad \overline{\mathcal{K}}^*=\int_0^\infty \overline{K}(t')dt' \ , \tag{8b}$$

$$A=4\pi\omega\eta''\frac{L_g}{L}\frac{1}{2k}D^0, \quad \overline{A}=4\pi\omega\overline{\eta''}\frac{L_a}{L}\frac{1}{2k}\overline{D^0} \ . \tag{8c}$$

Furthermore, we introduce some other quantities of interest in LSA theory as well in the following analysis:

$$a=\frac{I_{sg}}{I_{sa}}\ , \tag{8d}$$

$$\alpha_0=4\pi\frac{\omega}{c}\eta''D^0,\quad \overline{\alpha_0}=4\pi\frac{\omega}{c}\overline{\eta''}\,\overline{D^0}\ , \tag{8e}$$

$$\mathcal{B}_{sg}=4\pi\omega\eta''\frac{L_g}{L}\frac{1}{2k},\quad \mathcal{B}_{sa}=4\pi\omega\overline{\eta''}\frac{L_a}{L}\frac{1}{2k}\ , \tag{8f}$$

$$\mathcal{B}_g=\frac{4\pi\omega\eta''}{2k\hbar c}=\frac{\alpha_0}{\hbar\omega D_0}\frac{1}{2k},\quad \mathcal{B}_a=\frac{4\pi\omega\overline{\eta''}}{2k\hbar c}=\frac{\overline{\alpha_0}}{\hbar\omega\overline{D_0}}\frac{1}{2k}\ , \tag{8g}$$

$$A=\alpha_0\frac{L_g}{L}\frac{c}{2k},\quad \overline{A}=\overline{\alpha_0}\frac{L_a}{L}\frac{c}{2k}\ . \tag{8h}$$

Here $I_{sg}$ and $I_{sa}$ are, respectively, the gain-medium saturation intensity and the absorber-medium saturation intensity for a traveling wave and the factor of 2 in the denominator of Eq. (7) appears because of the standing-wave laser field. The constants $\mathcal{K}^*$ and $\overline{\mathcal{K}}^*$ are calculated in Appendixes B and C for particular choices of the level structure. The quantities $A$ and $\overline{A}$, with standard meaning in LSA theory, are defined as the ratio between the unsaturated small-signal gain or absorption and the cavity losses. At threshold of laser operation without any intracavity absorber the $A$ parameter is equal to 1. $\alpha_0$ and $\overline{\alpha_0}$ are the small-signal gain (unsaturated gain) and the small-signal absorption (unsaturated absorption) in the homogeneously broadened regime. The saturability parameter $a$ has the standard meaning of the ratio between saturation intensities of the gain and the absorber media. The parameters $\mathcal{B}_g$ and $\mathcal{B}_a$ are the stimulated emission coefficients normalized to the cavity damping rate and like the parameters $\mathcal{B}_{sg}$ and $\mathcal{B}_{sa}$ are determined by the emission and absorption coefficients $\eta''$ and $\overline{\eta''}$ of the molecules in the amplifier and absorber respectively. These quantities, as well as $A$ and $\overline{A}$, depend on the laser frequency through the $\eta''$ and $\overline{\eta''}$ dependencies reported in Eq. (2b).

Equation (7) shows that even in the case in which the relaxation depends on the dynamics of auxiliary levels, the steady-state equation of the LSA shows a stationary bistable behavior similar to that of the much more simplified models previously used to describe the LSA. The difference between previous models of LSA in $CO_2$ lasers and the present one consists mainly in the range of the parameters for which instabilities occur as well in the completely different dynamical scenario displayed by this new model. In the following sections we will discuss a modeling of the relaxation dynamics which will allow us to gain insight into the nature of the memory functions for the amplifier and the absorber.

## III. AMPLIFIER AND ABSORBER RELAXATIONS AND RATE-EQUATION MODEL

### A. Amplifier

The relaxation dynamics in carbon dioxide has been extensively studied by many authors and several models have been devised to explain the properties of a $CO_2$ laser, one main target being the comprehension of its high-gain saturation. An accurate investigation of the population dynamics in a $CO_2$ discharge has been recently reported using a probe diode laser resonant with some $CO_2$ levels.[7] The main feature of the relaxation dynamics consists in a very fast rotational relaxation of the radiation-excited level within the set of rotational levels belonging to a given vibrational band and by the slower vibrational-vibrational and vibrational-translational relaxations. However, the particular level configuration of the $CO_2$ molecule with quasidegenerate vibrational states and efficient energy pooling plays an important role in rendering the above mechanism peculiar to this kind of molecule. In the context of the LSA problem, as well in the dynamics of the $CO_2$ laser, the relaxation processes of the $CO_2$ amplifier have been modeled within the so-called four-level model,[13,2] where rotational coupling has been introduced, and later within a three-level model where the relaxation of the lower laser level towards the ground state has been added.[5] A rich complexity of behaviors has been obtained by the introduction of these additional relaxation processes.[14,15] By considering that the experimental investigations of the LSA display an even richer dynamical scenario, it is supposed that a full modeling of the relaxation processes would be capable of providing a closer agreement with experiments and perhaps new types of dynamical regimes.

The reduced model that we adopt merging the models of Refs. 2 and 5 is schematically represented in Fig. 1(a). The levels shown there represent sets of real $CO_2$ levels characterized by a fast relaxation rate within a given set. The relaxation toward external levels is a sort of weighted average of the relaxation rates for the single levels. The group denoted by 2 corresponds to the set of rotational states originating from the vibrational state $00^01$ and includes the upper laser level. The level 1 groups the rotational states corresponding to the vibrational states $10^00$, $02^20$, and $02^00$ which are strongly coupled by almost-resonant collisions. The level 0 contains the $01^10$ vibrational level and the $00^00$ ground state. The relaxation of the $01^10$ level towards the ground state, measured to be $3.3\times10^3\ \mathrm{sec}^{-1}\,\mathrm{Torr}^{-1}$ in a 1:9 $CO_2$:He mixture,[7(c)] may lead to a bottleneck phenomenon in the relaxation towards the ground state and will set an upper limit to the pumping rate for which the schematization of level 0 as a single level is valid. Figure 1(b), discussed in Appendix B, reports a model for the case where the schematization of a single level cannot be applied. We note that for the typical amplifier pressures, owing to the very fast rotational relaxation rates, an adiabatic elimination of the population of rotational levels can be applied.

### B. Absorber

The modeling of the absorption mechanism in the passive medium (we used mainly $SF_6$ as saturable absorber) involves some difficulties since the $SF_6$ infrared spectrum is very complex and several $\nu_3\leftarrow0$ lines fall within the absorption profile which, as a result of the low LSA working pressures, should be considered dominated by the Doppler broadening [half width at half maximum

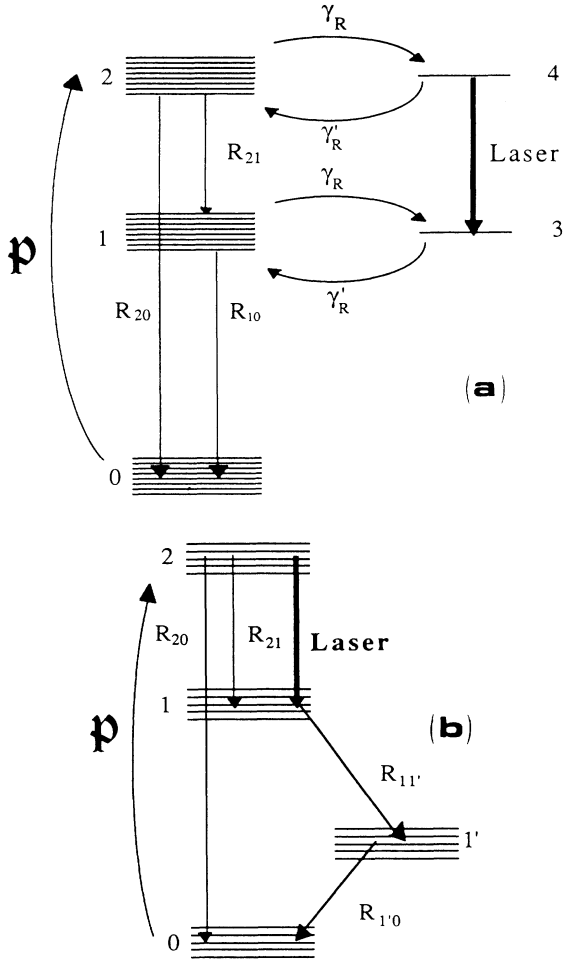


FIG. 1. Energy-level diagram of the amplifier medium including rotational-vibrational structure (a) within the model applied in this paper and (b) within a model taking care of the bottleneck phenomenon in the $1'=(01^10)$ level at high pumping of the $CO_2$ medium.

(HWHM) of 15.4 MHz at $T=300$ K]. For instance, from the saturated absorption measurements[16] it appears that for the line $P(16)$ at least four $SF_6$ transitions fall inside the Doppler profile, while for the $P(20)$ line one strong line with 27.7-MHz detuning and a weaker unassigned one with $-3.2$-MHz detuning interact with the laser transition. In our model we will avoid discussing in detail the relevance of these facts to the absorption mechanism of $SF_6$. Moreover, we will adopt a very crude schematization of the coupling with the radiation by setting up a system of rate equations for the set of molecules belonging to the velocity group tuned to the field. This will result in an absorption coefficient which correctly reproduces the Doppler absorption coefficient of the gas. However, the functional dependence of the saturation factor from the intensity will be the typical $(1+I/I_{sa})^{-1}$ dependence of a homogeneously broadened transition instead of the $(1+I/I_{sa})^{-1/2}$ dependence of an inhomogeneously broadened transition.

The absorber level diagram to be used in our modeling is shown in Fig. 2. The laser radiation is resonant with the two levels denoted by 2 and 4 which in turn are coupled via relaxation mechanisms to the rotational heat baths corresponding to the vibrational ground state level 1 ($v_3=0$) and excited level 2 ($v_3=1$), respectively.

### C. Rate equations

Following the previous considerations we can set up the system of rate equations for the intensity $I$ of the forward or backward wave in the cavity, and, corresponding to the level diagrams of Figs. 1(a) and (2) (see Appendixes B and C), for the population difference $D=(M_2-M_1)/N_{CO_2}$ between the amplifier upper and lower vibrational levels normalized to the population density $N_{CO_2}$, and for $\delta_R=(\overline{M_3}-\overline{M_4})/N_a$ the population difference between the absorber lower and upper rotational resonant levels normalized to the population density $N_a$. Making use of the memory functions, measuring the times in units of the cavity damping time $1/(2k)$, and normalizing the relaxation rates to the $2k$ rate, the rate equations are written

$$\dot{I}=I(B_{sg}D-B_{sa}\delta_R-1)\,, \tag{9a}$$

$$\dot{D}=2\mathfrak{P}\frac{R_{10}-R_{21}}{R_{20}+R_{10}+2\mathfrak{P}}-\left[\frac{R_{20}+R_{10}}{2}+R_{21}+4B_gI\right]D + \frac{R_{20}-R_{10}}{2}\left[\frac{R_{20}-R_{10}}{2}+R_{21}+\mathfrak{P}\right] \times\int_0^\infty \exp\left[-\left[\frac{R_{20}+R_{10}}{2}+\mathfrak{P}\right]t'\right]D(t-t')dt'\,, \tag{9b}$$

$$\dot{\delta}_R=-(\overline{\gamma_R}+4B_aI)\delta_R+\frac{\overline{\gamma_V}\,\overline{\gamma'_R}}{\overline{\gamma_V}+\overline{\gamma'_R}}\Delta_R^0 +\overline{\gamma_R}\,\overline{\gamma'_R}\int_0^\infty \exp[-(\overline{\gamma_V}+\overline{\gamma'_R})t']\delta_R(t-t')dt'\,, \tag{9c}$$

where we have made use of the parameters defined in the Appendixes.

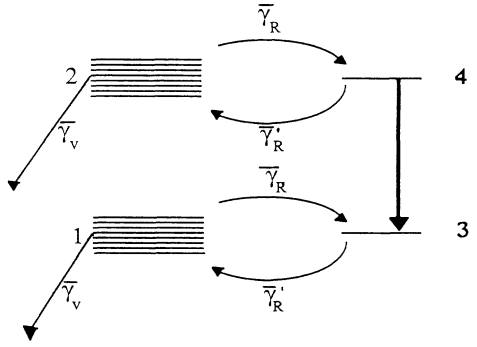


FIG. 2. Energy level diagram of the absorber medium including rotational and vibrational structures.

In the amplifier as well as in the absorber we have supposed the rotational relaxation constants of the upper level and lower level to be the same. In the amplifier an adiabatic elimination of the rotational levels has been applied; moreover, when this adiabatic elimination is performed,[2] a simplification may be introduced into the equations owing to the smallness of the transition rate induced by the radiation as compared to the level depletion due to rotational collisions.

Using Eqs. (9) and exploiting some relations derived in Appendixes B and C, we can explicitly calculate the parameters $A$, $\bar{A}$, and the saturation intensities of the amplifier and the absorber, which are given by

$$A = B_{sg} D^0 = B_{sg} \mathfrak{P} \frac{(1 - R_{21}/R_{10})}{R_{20} + R_{21} + \mathfrak{P}(1 + R_{21}/R_{10})} , \tag{10a}$$

$$\bar{A} = B_{sa} \delta_R^0 , \tag{10b}$$

$$I_{sg} = \frac{1}{B_g} \frac{R_{10}(R_{20} + R_{21} + \mathfrak{P}) + \mathfrak{P} R_{21}}{R_{20} + R_{10} + 2\mathfrak{P}} , \tag{10c}$$

$$I_{sa} = \frac{\bar{\gamma}_R}{2B_a} \frac{1}{1 + \dfrac{\bar{\gamma}'_R}{\bar{\gamma}_V}} . \tag{10d}$$

In the above equations $D^0$ represents the equilibrium value of the normalized population difference in the gain medium in absence of laser radiation and $\delta_R^0$ the normalized population difference between lower and upper absorber levels. Notice that $I_{sg}$ may be alternatively derived from Eq. (B3) for $\mathcal{H}^*$ making use of Eq. (8a) when, owing to the adiabatic elimination of the rotational population in Eq. (B3), the term with $1/\gamma'_R$ is neglected as compared to the other one.

In regard to the number of parameters effectively determining the dynamical behavior of Eqs. (9), we must note that only the ratio $B_a/B_g$ is important, the absolute value of $B_a$ and $B_g$ changing the intensity $I$ only by a multiplicative factor. Because in Eqs. (9) the typical $\mathfrak{P}$ values are very small compared to the relaxation rates in the amplifier the dependence of the memory function on the pumping rate $\mathfrak{P}$ can be neglected. We expect this to be true also in general therefore the influence of $\mathfrak{P}$ should be restricted only to the determination of the term $D^0$ in Eq. (1b). As a consequence only the product $B_{sg}\mathfrak{P}$, proportional to the parameter $A$, will determine the dynamical evolution of the intensity.

The form of Eqs. (9a) and (9b) for the variables $D$ and $\delta_R$ with memory functions allow us to make some comments on the roles played by the different relaxation rates in the LSA dynamics. It appears in Eq. (9b) that if $R_{10} = R_{20}$, the term containing the memory function disappears. Therefore the internal dynamics of the $CO_2$ amplifying medium becomes important owing to the differences in the vibrational relaxation rates of the two levels involved in the laser action. In Ref. 2 the LSA operation was investigated theoretically in the hypothesis of equal vibrational relaxation rates, so that the richness of the LSA dynamics could not be obtained. Asquini and Casagrande[17] examined the LSA operation for different vibrational relaxation rates but restricted their attention to the static operation and obtained no new results for the LSA dynamics. The numerical solution of the LSA equations with different vibrational relaxation rates was really started by Tachikawa *et al.*[5] who introduced at the same time the pumping from the ground state, whose role in the LSA dynamics is not relevant. Regarding the absorber dynamics, it appears from Eq. (9c) that the memory function has a range of influence on retarded times equal to $1/(\bar{\gamma}_V + \bar{\gamma}'_R)$, which is quite large. Therefore it should influence the slow LSA regimes as well as those unstable regimes emerging from a stationary solution, thus changing the stability ranges of the LSA.

## IV. EXPERIMENT

### A. Apparatus

The LSA apparatus, standard for intracavity experiments, is composed of a $CO_2$ laser ($L_g = 76$ cm) with a grating at one cavity end, an output mirror at the other end, and a central iris to realize the single-mode operation. It contains an intracavity ($L_a = 45$ cm) cell where different absorbing gases, at pressures in the 20–50-mTorr range, are injected in a flowing regime. The current in the discharge tube containing the gases at 19 Torr total pressure in the ratio $CO_2$:$N_2$:He, 1:1.5:5, is stabilized to an high degree. The cavity damping time, measured by introducing into the intracavity cell an unsaturable absorber,[18] was $2k = 2.3 \times 10^7$ sec$^{-1}$. The main improvement in the experimental arrangement, described in detail in previous papers,[19,20] was in the data recording and handling. Thus the signal at the detector output corresponding to the static regime or produced by the laser pulses in the unstable and chaotic regimes were recorded directly by a PC microcomputer or on a transient digitizer, whose output was transferred to the PC microcomputer. The records of time evolutions, phase portraits for the laser pulses, first-passage times, return maps of the intensity, and of the return time were obtained through an analysis of the data stored in the computer. Return times and statistical fluctuations in the return times were obtained by recording up to 200 laser pulses in the microcomputer memory.

The laser evolution was monitored as a function of the control parameter: the $CO_2$ amplifier current, the absorber pressure, and the laser frequency detuning $\delta\nu = (\omega - \omega_0)/2\pi$ within the mode contour. The laser current is related to the pumping in the amplifier, i.e., to the $A$ parameter. By measuring the laser output power as a function of the current $i$ flowing through the discharge and comparing it with the theoretical description, the functional relation connecting the laser parameter $A$ to the discharge current is determined. In Fig. 3 we report a typical result for the output intensity $I_{\text{out}}$ of the laser when the intracavity cell did not contain a saturable absorber. The output intensity $I_{\text{out}}$ is related to the control parameter $A$ and the saturation intensity $I_{sg}$ through the following relation:

$$I_{\text{out}} = T I_{sg} (A - 1)/2 , \tag{11}$$

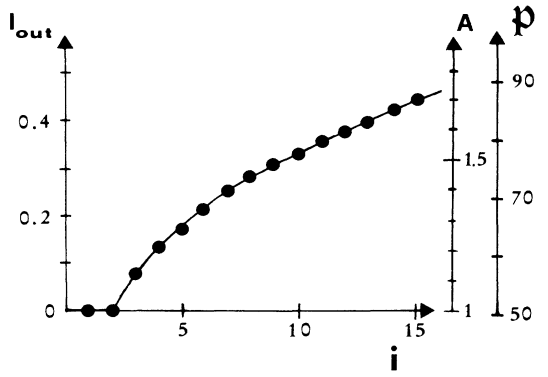


FIG. 3. Plot of the measured laser output intensity $I_{out}$ (measured in W/cm$^2$) vs the current $i$ (measured in mA) in the amplifier for the $10P(20)$ laser line without the intracavity absorber; the vertical scales on the left report the $A$ and $P$ (in sec$^{-1}$) parameters as derived from a fit of the measured output intensity. Error bars on the current and the output intensity are smaller than the dot dimensions.

with the output mirror transmissivity $T=0.03$. This relation allows us to establish a mapping between the parameter $A$ and the discharge current once the value of $I_{sg}$ is known and does not change appreciably with the discharge current. This last condition has been verified for our laser system in Ref. 19. The value of the saturation intensity, previously measured to be $I_{sg}=40$ W/cm$^2$ using a nonsaturable absorber,[18] is reproduced by the data of Table I using Eq. (10c), where the $\mathfrak{P}$ terms can be neglected. By using the experimental results of Fig. 3, we have determined the functional dependence of the pumping rate $\mathfrak{P}$, measured in sec$^{-1}$, from the laser discharge current to be

$$\mathfrak{P}=51+6.9(i-2.0)^{0.65}\ , \tag{12}$$

where $i$ is measured in mA. It should be noticed that the functional dependence of the pump parameter $\mathfrak{P}$ on the current is different from that of Ref. 5. In fact the current dependence of the $\mathfrak{P}$ parameter is determined by the internal structure of the $CO_2$ amplifier and that structure, probably not completely described by the three-level model of the amplifier, does not give equal result in the two experiments.

### B. LSA parameters

We summarized in Table I the parameters characteristic of our LSA experiments with $SF_6$ and $^{15}NH_3$. The relaxation of the upper $CO_2$ laser level $R_{20}$ characterized by slow vibrational-vibrational, vibrational-translational deexcitation and diffusional processes, has been measured as $5.5\times10^3$ sec$^{-1}$ for a typical laser mixture at 10-Torr pressure and 20-mA discharge current.[7(c)]. A slightly different value has been inserted in Table I in order to fit the experimental value for the saturation intensity $I_{sg}$. The relaxation $R_{10}$ of the lower laser level, as measured in (7c), has a value of $1.3\times10^6$ sec$^{-1}$ for our working pressure. The relaxation rate $R_{21}$ is very small: its value can be taken to be $\sim10$ sec$^{-1}$ on thermodynamic bases and its role in the dynamics of the amplifier is negligible. The $CO_2$ rotational relaxation rate $\gamma_R$, measured by Degnan,[21] for our mixture and pressure is $2.5\times10^8$ sec$^{-1}$.

While in the experiment use was made of several absorbing gases, most theoretical attention was given to the $SF_6$ experiments. The decay times of rotational levels in $SF_6$ have been reported by Moulton *et al.*[22] for the excited and ground vibrational states. In our model these times are assumed to be equal; therefore we adopt a rotational relaxation rate of $2.9\times10^7$ sec$^{-1}$ Torr$^{-1}$. At small

TABLE I. Parameters for our LSA with 25-mTorr $SF_6$ or 10-mTorr $^{15}NH_3$ absorber. The values for $SF_6$ have been derived from Refs. 16, 22, and 24 and that corresponding to $^{15}NH_3$ from Ref. 25. Relaxation rates are measured in units of $2k=2.3\times10^7$ sec$^{-1}$, the cavity damping rate.

| | Line | | |
|---|---|---|---|
| | $10P(20)$ | $10P(16)$ | $10R(42)$ |
| | Amplifier ($CO_2$) | | |
| $B_{sg}$ | $1.5\times10^2$ | $1.5\times10^2$ | 48 |
| $B_g$ (W$^{-1}$ cm$^2$) | $0.8\times10^{-5}$ | $0.8\times10^{-5}$ | $2.4\times10^{-6}$ |
| $R_{10}$ | 0.056 | 0.056 | 0.056 |
| $R_{20}$ | $3.5\times10^{-4}$ | $3.5\times10^{-4}$ | $3.5\times10^{-4}$ |
| $R_{21}$ | $4.0\times10^{-7}$ | $4.0\times10^{-7}$ | $4.0\times10^{-7}$ |
| $\gamma_R$ | 10.4 | 10.4 | 10.4 |
| $\gamma'_R$ | 0.68 | 0.68 | 0.68 |
| | Absorber | | |
| | $SF_6$ $\nu_3$ $P(59)$, $A_2$ | $SF_6$ $\nu_3$ $Q(38)$, $F_2+E+F_1$ | $^{15}NH_3$ $\nu_2$ $^{as}R(2,0)$ |
| $\overline{\delta\nu}$ (MHz) | 27.7 | $-7.25$ | 52.0 |
| $\overline{A}$ | 0.49 | 8.9 | 10.1 |
| $\overline{B_a}$ (W$^{-1}$ cm$^2$) | 3.4 | 2.24 | 2.0 |
| $\overline{\gamma_R}$ | 0.032 | 0.032 | 0.036 |
| $\overline{\gamma'_R}$ | $1.6\times10^{-5}$ | $1.18\times10^{-4}$ | $9.6\times10^{-4}$ |
| $\overline{\gamma_V}$ | $1.31\times10^{-3}$ | $1.31\times10^{-3}$ | $1.31\times10^{-3}$ |

absorber pressures as ours (25 mTorr), the vibrational relaxation time is principally determined by transit time across the laser beam (0.3 cm diameter). This relaxation process is taken into account by introducing a $4.0\times10^4$ $sec^{-1}$ relaxation rate for the $\overline{\gamma_V}$ vibrational relaxation of the absorber.

The parameters $B_{sg}$, $B_g$, $B_{sa}$, and $B_a$ describing the interaction between laser field and amplifier and absorber media have been derived from Eqs. (8), (B5), and (C2) as a function of the experimentally determined absorption coefficients by using the molecular constants and the level structure available in the literature for the $CO_2$ amplifier,[23] for $SF_6$,[22,24] and for $^{15}NH_3$.[25] The absorber parameters have been calculated for a laser tuned at the center of the cavity mode [$\delta\nu=(\omega-\omega_0)/2\pi=0$] and in Table I the detuning $\overline{\delta\nu}$ indicates the frequency of the nearest assigned absorption line. The absorption coefficients refer to inhomogeneous broadening and the homogeneous linewidth results equal to the inhomogeneous one for an absorber pressure roughly 0.5 Torr.

## V. EXPERIMENTAL STATE DIAGRAM

We have investigated the LSA regimes as a function of the control parameters. A typical result for the LSA output intensity versus the pump control parameter $A$ is reported in Fig. 4, obtained from the PC recorded data. The LSA output, obtained for the $10P(16)$ $CO_2$ line and $SF_6$ absorber at 12 mTorr with 500-mTorr $N_2$ buffer gas, presents, as $A$ is increased, initially the off regime, later a pulsed regime, and finally the cw regime corresponding to an intensity $I_+$ [Fig. 4(a)]. On the contrary, when the $A$ pump parameter is decreased, Fig. 4(b), the pulsed region appears on a more narrow region as a consequence of the bistability between cw and pulsed regimes displayed by the LSA. The pulsed regimes, generally denoted as PQS, have been classified in Refs. 15 and 8 as type-I quasihomoclinic orbit and cycle instabilities, and type-II instabilities. The pulses reported in Fig. 4 are classified as quasihomoclinic orbits in type-I instabilities. The experimental results of Fig. 4 have been obtained in a regime of homogeneous broadening due to the presence of the $N_2$ buffer gas.

The result of the investigations of LSA operating regimes may be presented on a state diagram as a function of the control parameters, as shown in Figs. 5–7 for different LSA operations. Figure 5 refers to the $CO_2$ operations on the $10P(16)$ line with an $SF_6$ absorber and reports the operation regimes at a constant absorber pressure (20 mTorr) as a function of the pump parameter and the laser frequency parameter $\delta\nu$. The state diagram shows the presence of generalized bistability between PQS type-II and off regimes. Each state diagram has been explored vertically, i.e., keeping constant the control parameter plotted on the horizontal axis. Quite different bistability ranges may be obtained when the operation is modified, i.e., by keeping constant the vertical control parameter and by scanning the horizontal parameter. A similar diagram for the $10P(20)$ line with 25-mTorr $SF_6$ absorber is reported in Fig. 6. The LSA operation reports type-I PQS regions with extensions depending on the absorber pressure and the laser detuning. The $10P(16)$ and $10P(20)$ lines produce quite different results even if the $SF_6$ absorption coefficient is very similar in order of magnitude, probably as a consequence of different frequency tunings in respect to the several transitions contributing to the $SF_6$ absorption coefficient on those $CO_2$ laser lines. The centers of $SF_6$ absorption lines have been plotted in Figs. 5 and 6.

An important question concerning the analyses of the LSA experiments is that most observations are performed with a low-pressure saturable absorber, thus in a regime of inhomogeneously broadened transition line. However, we have noticed that by adding a buffer gas to a low-pressure absorber, in such a way that the line becomes homogeneously broadened, the range of bistability and PQS operations for the LSA is not greatly affected. Experimental evidence of this behavior is the comparison between Fig. 4 and Figs. 5 or 6, because Fig. 4 reports

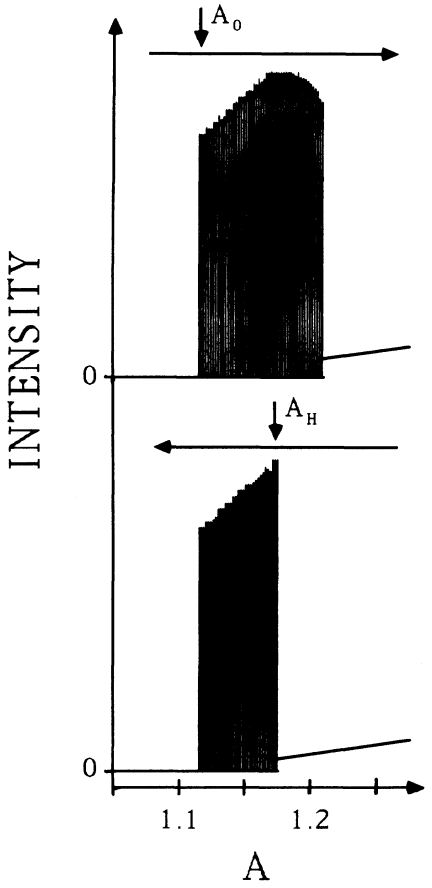


FIG. 4. Laser output intensity vs the $A$ pump parameter for the LSA operations on the $10P(16)$ $CO_2$ line with 12-mTorr $SF_6$ absorber and 500-mTorr $N_2$ buffer gas as obtained through a reconstruction of the computer-recorded data. The regions of dark vertical lines indicate pulsing regimes, and the extrema of the vertical lines represent the maximum intensities of the pulses. The $A_O$ and $A_H$ values are reported on the horizontal axes.

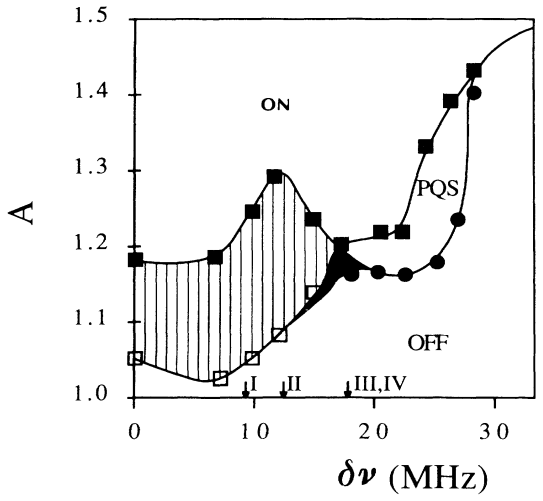


FIG. 5. LSA state diagram in the $(A,\delta\nu)$ plane for the $10P(16)$ line and $SF_6$ at 20 mTorr, presenting off, cw and PQS operations, with bistability between cw and off operations in the dashed area and bistability between PQS and off operations in the darkened area. The data were obtained by sweeping $A$ at constant $\delta\nu$. The arrows, marked I–IV on the horizontal scale, denote the center frequency of the $Q(43)F_1$, $Q(45)F_2$, $Q(43)E$, and $Q(48)F_2$ $SF_6$ absorption lines, as measured in Ref. 16. The continuous lines through the experimental points have been drawn only for clarity of presentation.

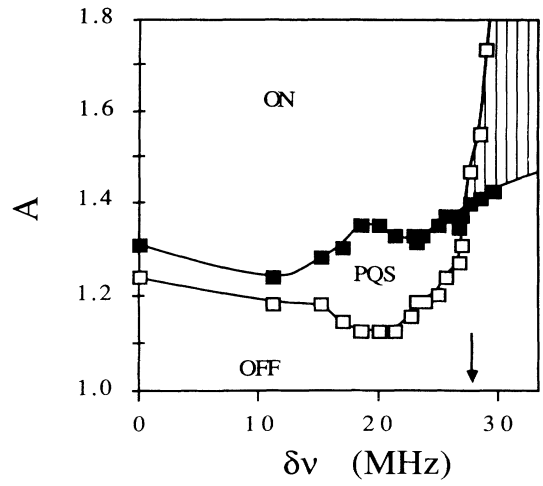


FIG. 6. Same diagram as in Fig. 5 for $10P(20)$ and $SF_6$ at 25 mTorr, with bistability between cw and off operations in the dashed area and bistability between PQS and off operations in the darkened area. The data were obtained by sweeping $A$ at constant $\delta\nu$. The arrow on the horizontal scale denotes the center frequency of the $P(59)A_2$ $SF_6$ absorption lines, as measured in Ref. 16. The continuous lines through the experimental points have been drawn only for clarity of presentation.

$SF_6$ data with buffer gas at a pressure giving homogeneous broadening and Figs. 5 and 6 represent the $SF_6$ data in an inhomogeneously broadened regime. It results that the range of $A$ values producing bistability and pulsation is similar in both cases.

## VI. COMPARISON WITH $SF_6$ EXPERIMENTAL RESULTS

We have performed a comparison of experimental and theoretically calculated laser intensity-switching points characterizing a given LSA stationary behavior. We

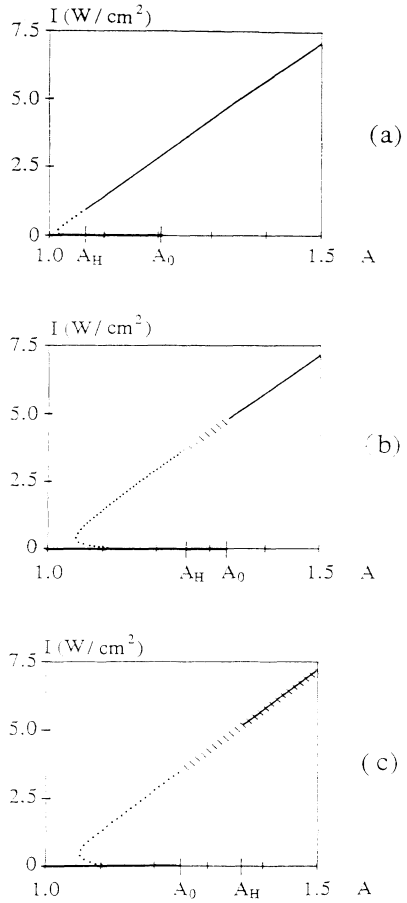


FIG. 7. Theoretical results for the intracavity laser intensity $I$ vs the $A$ control parameter for $SF_6$ absorber on the $10P(16)$ and $10P(20)$ lines at 25-mTorr pressure in (a) and (b), respectively, and in (c) on the $10P(16)$ line for a homogeneous broadening of 25-mTorr absorber owing to buffer gas collisions. For (a) and (b) the relaxation rates are in Table I and the $B$ parameters, as indicated in the text, have been chosen to reproduce the experimentally observed $A_O$ and $A_H$ values. For (c) $B$ parameters come from fitting the experimental observations and $\overline{\gamma_R}=0.64$ and $\overline{\gamma'_R}=2.4\times10^{-3}$ for collisions with $N_2$ buffer gas. ——, regions of stable solutions; \ \ \ \, PQS type-I instability regions; · · · ·, solutions inaccessible experimentally. Notice that in (c) a generalized bistability between cw and PQS operations is obtained for all the reported $A$ values larger than $A_H$.

have in fact examined the values of $A_O$ and $A_H$. $A_O$ is the value of the pumping parameter corresponding to the threshold for the laser oscillation whereas $A_H$ is the Hopf bifurcation value at which the nontrivial stationary solution of Eqs. (9), stable for higher values of $A$, loses its stability by making a transition to either a state of zero intensity or to a regime of PQS. The theoretical results of Fig. 7, obtained as fit to the experimental observations, present the $A_O$ and $A_H$ values in different operating regimes. For bistability between two cw steady states [Fig. 7(a)], $A_O$ and $A_H$ delimit the bistability region. In presence of PQS regimes $A_O$ and $A_H$ denote where the cw steady states lose their stability, as in the experimental observations of Fig. 4. The $A_O$ value is directly connected to the parameter $\bar{A}$ through the relation $A_O=1+\bar{A}$, which in turn is related to the small-signal absorption coefficient of the $SF_6$ according to Eq. (8). $A_H$ can be calculated by applying a stability criterion to the solution $I_+$.

We have found experimentally $A_O=1.22$ for the LSA operation on line $10P(16)$ with 25-mTorr $SF_6$ and $A_O=1.26$ for operation with $10P(20)$ line corresponding to $\bar{A}=0.22$ and $\bar{A}=0.26$, respectively. However, these values do not agree with those reported in Table I, calculated by making use of the well-established absorption coefficients for $SF_6$ corresponding those laser lines. A legitimate doubt is that this disagreement could originate in an incorrect value of $I_S$ or the cavity damping $k$. However, it is highly improbable that these could account for discrepancy of about one order of magnitude or more. In any case we observe that the ratio between the two values of $\bar{A}$, which does not suffer from the uncertainties in $I_S$ and the cavity damping $k$, does not equal the ratio between the absorption coefficients corresponding to the two laser lines. We have decided to use these $\bar{A}$ parameters as adjustable parameter for our model. If we turn now our attention to the experimentally determined value of $A_H$ we note that $A_H\cong 1.3$ for the LSA working on the $10P(20)$ line and $A_H\cong 1.06$ for LSA on $10P(16)$. By making use of our model and applying a stability criterion to the solution $I_+$ we determine instead for both laser lines a value of $A_H$ which is very close to unity. We find that, in order to reproduce the experimental values of $A_H$, we must modify the values of $B_a$ with respect to those found in Table I; the values which correctly reproduce $A_H$ are $B_a=1.52$ and $0.22\ W^{-1}cm^2$ for $10P(16)$ and $10P(20)$ lines, respectively. Figures 7(a) and 7(b) report the solutions given by the model for those two lines using the $\bar{A}$ and $B_a$ parameters as free variables to reproduce the experimental phase diagrams. We note here that the calculated values of $B_a$ give a very low value of the saturation intensity of the absorber and therefore it is to be expected that the stationary solution becomes unstable only for $A$ values very close to 1 which, on the other hand, is not the case of the experimental results. It is clear therefore that probably the main source of disagreement with LSA experiments resides in the modeling of the absorber which at low pressures could interact with the radiation in a very complicated and nonstandard way. We will discuss in the following some features that we have neglected in our model and that can be responsible for the disagreement with the experiment.

The first one consists of having considered a homogeneous broadened feature for $SF_6$ absorption, whereas, at the very low pressures at which the LSA operates, this absorber presents a Doppler broadened absorption line. On the other hand, the results of Fig. 4, relative to operation of the LSA with a homogeneously broadened $SF_6$ absorber (due to collisions with $N_2$ buffer gas), can be reproduced by supposing the rotational relaxation rates by collisions with $N_2$ are the same as for collisions with $SF_6$ and using $B_{sa}=0.24\ W^{-1}cm^2$ and $B_a=0.11\ W^{-1}cm^2$ [see Fig. 7(c)]. Thus very similar results seem to appear for interaction of the radiation with a narrowly delimited velocity group of molecules, as in the inhomogeneous broadening case, and for interaction with the total velocity distribution, as in the homogeneous case. We deduce that in the experiment the velocity diffusion processes play an important role in influencing the absorption mechanism and in particular by raising the value of the saturation intensity, which from Eq. (10d) is inversely proportional to $B_a$. In fact the presence of efficient elastic velocity changing collisions in $SF_6$ has been demonstrated[26] with a $5\times 10^5\ sec^{-1}$ collision rate at 25-mTorr working pressure, a rate fast in comparison to other absorber rates of Table I.

A second approximation probably derives from some peculiar features concerning the absorption of infrared radiation by $SF_6$ which have not been included in our model. It is well known that owing to the low anharmonicity of the $SF_6$ vibrations the absorbed radiation can be at the same time resonant with a hot-band vibrorotational transition. This mechanism could have some influence on the incorrect reproduction of the $A_H$ value in our model. Although some authors[27] have considered this phenomenon, their experimental measurements have relied on rate equation models in which, according to our opinion, overly drastic simplifications were made. It appears, therefore, that even if the excited-state absorption plays an important role, a more complex modeling of the absorption mechanism should be carefully considered, at least for the $10P(20)$ line, which is more affected by the multiple absorption as compared with the $10P(16)$ line.

As a last possibility we should consider that another mechanism, of a completely different nature than that emerging from the rate-equation approach, could be responsible for the discrepancies in the values of $A_O$ and $A_H$. As noticed above the frequency of the laser can be perturbed when the absorber is placed in the cavity and this influence can also affect the dynamic regime of the LSA. The importance of laser-detuning effects for the different LSA solutions has been pointed out recently.[28] In such a case, the picture resulting by considering the various $SF_6$ lines falling within the laser profile would become a very difficult one to handle from the theoretical point of view. In this case a more simple absorbing system such as $NH_3$ should be considered for theoretical investigations. However, in order to describe these effects we should complement our system of equations with an additional one taking into account the optical path of the

radiation inside the cavity.

Finally it should be noticed that the LSA experiments analyzed in this paper are performed in a regime where the uniform-field approximation cannot be properly applied. In Ref. 18 it was shown how the LSA bistable regime can be described without the uniform-field approximation, but the resulting rate equations appear rather intractable. Thus in the present paper the uniform-field approximation has been used to analyze the experimental results, even if parameters such as the cavity damping rate have been derived from the static regime without that approximation.[18]

## VII. CONCLUSIONS

We have presented an LSA model that takes into account the internal structure of the amplifier and absorber media. Introducing a memory function in the equation for the population difference interacting with the laser radiation makes it possible to describe in a unified way the molecular complexities. Specific applications have been presented in describing the rotational-vibrational structure, the pumping action from the ground state to the upper lasing level in the $CO_2$ laser, or both structures combined. The memory function approach allows consideration, in a unified way, of all level schemes with a rather complicated structure.

Some experimental results concerning the LSA regimes for different intracavity absorbing gases have been presented. Additional results concerning the LSA unstable and chaotic regimes will be presented in Ref. 8. The main interest of the present paper was a comparison of the model with the experimental results for the LSA operations. In fact we have been able to gain insight into the mechanism of the LSA response in the bistability and pulsation regimes. This analysis should be compared to that made by Tachikawa *et al.*[14(c)] on the basis of a slightly different model. The main difference between the model used in that work and that presented here consists in the inclusion in the present model of the rotational-vibrational structure of the absorber. On the contrary in Refs. 14 the absorber internal structure was simplified to a single rotational relaxation rate. An adiabatic elimination of the absorber rotational population may be applied at high absorber pressures (or high buffer gas pressures). At low absorber pressures the rotational structure is an important component in the description, and by neglecting it a wrong estimate is obtained for the saturation intensity and the locations of different regimes in parameters space. The analyses of Ref. 14 were based on the absorber rotational population difference without including the vibrational structure and the vibrational relaxation. In fact the pump control parameter was used as a free parameter in the analysis of Tachikawa *et al.*, whereas in our analysis it was fixed by the laser response without the intracavity absorber. An important result coming from the memory-function approach is that the important role played by the internal dynamics of $CO_2$ is not associated with the three-level pumping mechanism, as appeared from the numerical analysis of Ref. 14, but is associated with the different vibrational relaxation rates of the lasing levels.

In the present LSA model, as well in the large majority of previous works, a homogeneous broadening of the absorber has been assumed in deriving the LSA rate equations, even if in most experiments a low-pressure absorber is used, giving inhomogeneously broadened lines. However, an important experimental result of the present paper is that by adding a buffer gas, and thus passing to a homogeneously broadened regime, the ranges of bistable or unstable regimes are modified by less than 20%. In fact our model has been properly applied to the LSA observations with a homogeneously broadened line. However, it turned out that the observations of homogeneous broadening as well as the LSA fixed points in the inhomogeneous broadening case could not be fitted on the basis of the absorption coefficients available from the literature. Thus in our analysis the strengths of the laser-absorber interaction parameters were used as adjustable parameters. A result coming from our modeling is that the velocity diffusion in the absorber is probably playing an important role in determining the LSA operation. Thus at the present stage, where without introducing *ad hoc* parameters the state diagram cannot be reproduced within a 50% range of values, the application of a homogeneously broadened theory is a satisfactory approach. The question of a suitable model for the saturation of molecular gases used as saturable absorbers in the infrared has been investigated in detail in the past.[13(a),29] Beside the rotovibrational structure, other features have been included in those models, such as the spatial diffusion of the molecules, the temperature gradient, and the distortion of the optical beam, whose importance depend on the geometry and pressure of the absorber. It is very difficult to include those features in our LSA description. Furthermore, in our opinion the laser frequency detuning and the excited-state absorption play the most important role in the discrepancies between the theoretical parameters and the fitted ones. An important result arising from the theoretical model of Ref. 13(a) is that at laser intensities comparable to those of LSA intracavity experiments, the $SF_6$ saturation behavior may be treated as a homogeneous one with saturation larger than that predicted by a simple two-level model, in agreement with the result of this paper.

Frequency detuning and transverse distribution of the laser field have been left out of the analysis. In the future we plan to investigate theoretically and experimentally the role of the laser frequency. The analysis of the stationary regime for our LSA according to the above suggestions is currently under investigation and the results of this inquiry will be published in a forthcoming paper.

## ACKNOWLEDGMENTS

The authors wish to thank N. B. Abraham, D. Dangoisse, M. Tachikawa, and K. Tanii for fruitful discussions, and C. Gabbanini and E. Menchi for participation in some measurements. The work was performed within the Dynamics of Nonlinear Optical Systems Twinning Program of European Economic Community, and one of us (D.H.) would like to thank the European Economic Community for financial support.

## APPENDIX A: MEMORY FUNCTION

We present here, by exploiting the linearity of the relaxation mechanism associated with the variable difference of population of the tuned transition, a method for deriving the general laser equations given in Sec. II. For such purpose we give a short review of the standard theory of memory functions as it is used in the solution of systems of first-order linear differential equations. We start by considering the following system of linear differential equations with an external forcing $f_i(t)$:

$$\dot{x}_i = \sum_{j=1}^{N} \mathcal{A}_{ij} x_j + f_i(t) , \tag{A1a}$$

which can also be written in the more compact vectorial notation as

$$\dot{\mathbf{x}} = \underline{\mathcal{A}}\mathbf{x} + \mathbf{f}(t) . \tag{A1b}$$

When referring to our specific problem, the variables $x_i$ will be identified with the populations of our level system and the $A_{ij}$ with either relaxation or pumping rates or a combination of both. The role of the term $f_i(t)$ will become clear in the course of the present derivation.

The standard theory of linear differential equations gives the solution of Eq. (A1) in the following form:

$$\mathbf{x}(t) = \mathbf{x}(0)\exp(\underline{\mathcal{A}}t) + \int_0^t \exp(\underline{\mathcal{A}}s)\mathbf{f}(t-s)ds . \tag{A2}$$

We note that as long as the matrix $\underline{\mathcal{A}}$ satisfies the condition

$$\lim_{t\to\infty} \exp(\underline{\mathcal{A}}t) = 0 , \tag{A3}$$

for times large enough that the term $\exp(\underline{\mathcal{A}}t)$ can be considered small, the solution can be written as follows:

$$\mathbf{x}(t) = -\int_0^\infty \underline{K}(s)\mathbf{f}(t-s)\cdot d\mathbf{s} , \tag{A4}$$

with $\underline{K}(t) = -\exp(\underline{\mathcal{A}}t)$. We note here that the condition (A3) holds if the eigenvalues of the matrix $\underline{\mathcal{A}}$ are all negative, which is obviously satisfied in our case. As a final remark we observe that the matrix $\underline{K}$, which usually is named the "memory matrix," satisfies the following differential equation:

$$\dot{K}_{is} = \sum_{j=1}^{N} \mathcal{A}_{ij} K_{js}, \quad K_{is}(0) = -\delta_{is} . \tag{A5}$$

The above equation illustrates a very important property of the memory matrix: $\underline{K}$ is determined only by the free evolution of the system. In particular we see that the $s$th column can be identified with a vector satisfying Eq. (A1) with $f_i(t) = 0$ and initial conditions $x_i(0) = -\delta_{is}$.

Let us consider now the evolution of a variable $x_1$ ruled by a nonlinear term pumping term $\mathcal{P}(x_1,t)$ and coupled linearly to a set of other $n-1$ variables $x_2, \ldots, x_n$. These equations can be written as follows:

$$\begin{aligned} x_1 &= \mathcal{A}_{11}x_1 + \mathcal{A}_{12}x_2 + \mathcal{A}_{13}x_3 + \cdots + \mathcal{A}_{1n}x_n + \mathcal{P}(x_1,t) , \\ x_2 &= \mathcal{A}_{21}x_1 + \mathcal{A}_{22}x_2 + \mathcal{A}_{23}x_3 + \cdots + \mathcal{A}_{2n}x_n , \\ &\cdots \\ x_n &= \mathcal{A}_{n1}x_1 + \mathcal{A}_{n2}x_2 + \mathcal{A}_{n3}x_3 + \cdots + \mathcal{A}_{nn}x_n . \end{aligned} \tag{A6}$$

The vector $(x_2, x_3, \ldots, x_n)$ can be found in terms of the variable $x_1$ by using Eq. (A4). After inserting in the first equation the expressions for $x_2, \ldots, x_n$ as a function of $x_1$ we arrive at the final equation

$$\dot{x}_1 = \mathcal{A}_{11}x_1 - \int_0^\infty K'(s)x_1(t-s)ds + \mathcal{P}(x_1,t) , \tag{A7}$$

or by absorbing the first term at the second member into the memory function in the form of a $\delta$-function-term

$$\dot{x}_1 = -\int_0^\infty K''(s)x_1(t-s)ds + \mathcal{P}(x_1,t) . \tag{A8}$$

As opposed to the case of the memory matrix of Eq. (A4), the memory function of Eq. (A8) has a different meaning in terms of the free evolution of the system represented by the matrix $\underline{\mathcal{A}}$. In fact the evolution for the memory function $K'$ is that of the subsystem represented by the element $\mathcal{A}_{11}$ of the matrix $\underline{\mathcal{A}}$. Thus $K'$ represents the contribution into the first equation of the set (A6) of all the other variables different from $x_1$ when they evolve uncoupled from $x_1$. This contribution must be evaluated on a free evolution ruled by $\mathcal{A}_{11}$ with initial conditions $x_i(0) = -\mathcal{A}_{i1}$ $(i = 2,n)$.

A useful quantity is the integral $\mathcal{K}^*$ of the memory function, which as we have seen appears in Eqs. (8). To find it let us consider Eq. (A8) with a constant $\mathcal{P}$ term independent of the time. The solution will be given by

$$x_1 = \frac{\mathcal{P}}{\int_0^\infty K(t')dt'} . \tag{A9}$$

Equivalently, by solving the linear equation resulting from Eqs. (A6) it is obtained:

$$x_1 = -\mathcal{P}\frac{\|\mathcal{A}_{11}\|}{\|\underline{\mathcal{A}}\|} . \tag{A10}$$

By comparison of Eq. (A9) and Eq. (A10) we find

$$\mathcal{K}^* = \int_0^\infty K(t')dt' = -\frac{\|\underline{\mathcal{A}}\|}{\|\mathcal{A}_{11}\|} , \tag{A11}$$

which indicates a way to obtain $\mathcal{K}^*$ by making use of Eq. (A10) for $x_1$ when a unitary source $\mathcal{P} = 1$ is given to this variable in Eqs. (A5).

## APPENDIX B: RELAXATION DYNAMICS IN THE AMPLIFIER

We present the relaxation scheme used for the amplifier medium and apply it to the calculation of the memory function and of the saturation intensity for this medium through Eq. (8a). We need thus to compute the memory-function integral corresponding to the variable population difference for the radiation resonant rotational levels of the amplifier. In the level diagram of Fig. 1(a) these levels are defined as 3 and 4 and are coupled to the

vibrational manifolds 2 and 1 through rotational relaxation rates. We will suppose that upper and lower levels have equal rotational relaxation rates. Figure 1(a) reports the relaxation and pumping mechanism in the amplifier medium as adopted in our model. The populations $M_4$ and $M_3$ are those of the levels tuned to the radiation, and $M_4-M_3$ the relevant variable for which the memory function should be determined. If the total population of $CO_2$ vibrational levels $M_1$ and $M_2$ are defined excluding $M_3$ and $M_4$, respectively, the rate equations for this set of levels, with times measured in units $1/(2k)$ of the cavity damping time and relaxation rates normalized to $2k$, are given by

$$\begin{aligned}
\dot{M}_4 &= -\gamma_R M_4+\gamma'_R M_2-2\mathcal{B}_g I(M_4-M_3)\ ,\\
\dot{M}_3 &= -\gamma_R M_3+\gamma'_R M_1+2\mathcal{B}_g I(M_4-M_3)\ ,\\
\dot{M}_2 &= -(R_{21}+R_{20}+\mathfrak{P})M_2-\mathfrak{P}M_1+\gamma_R M_4\\
&\quad -\gamma'_R M_2+\mathfrak{P}N_{CO_2}\ ,\\
\dot{M}_1 &= -R_{10}M_1+R_{21}M_2+\gamma_R M_3-\gamma'_R M_1\ .
\end{aligned} \tag{B1}$$

$\mathfrak{P}$ is defined as the pumping rate from the ground vibrational manifold 0 to the upper vibrational manifold 2. $R_{ij}$ denotes the relaxation rate from the $i$ vibrational manifold to the $j$ vibrational manifold. $\mathcal{B}_g$ defines the absorption coefficient coupling of levels 3 and 4 with the radiation of intensity $I$. The ratio $\gamma'_R/\gamma_R$ between rotational relaxation rates is found on the basis that the equilibrium between the populations of the rotational levels, as determined by Eqs. (B1) in absence of the laser field, satisfies the Boltzmann distribution. Thus the ratio $\gamma'_R/\gamma_R$ is equal to the Boltzmann exponential factor divided by the rotational partition function.[13] In Eqs. (B1) we have supposed that the lower and upper states have nearly equal Boltzmann exponential factors. Following the procedure outlined in Appendix A we can find $\mathcal{H}^*$ by eliminating the terms containing the radiation in Eqs. (B1), the constant $\mathfrak{P}$ term, and putting a source term $\frac{1}{2}$ to $M_4$ and $-\frac{1}{2}$ to $M_3$ in the resulting stationary equations. By solving the resulting equations we find

$$\mathcal{H}^*=\frac{2\gamma_R/\gamma'_R}{\dfrac{1}{\gamma'_R}+\dfrac{R_{10}+R_{20}+2\mathfrak{P}}{\mathfrak{P}R_{21}+R_{10}(R_{20}+R_{21}+\mathfrak{P})}} \tag{B2}$$

and the saturation intensity is given by $I_{sg}=\mathcal{H}^*/(2\mathcal{B}_g)$.

In the $CO_2$ model of Fig. 1(a) a simplification was introduced to incorporate the $01^10$ manifold with the 0 together with the ground state $00^00$, owing to the fast relaxation rate between those levels. A better description is obtained by separating those two vibrational manifolds. For the typical values of pressure used in the $CO_2$ amplifier media, an adiabatic elimination of the rotational variables can be applied, so that the simple model of Fig. 1(b) with vibrational population only may be applied to describe the amplifier. For that level diagram we can write the following set of equations:

$$\begin{aligned}
\dot{M}_4 &= -\gamma_R M_4+\gamma'_R M_2-2\mathcal{B}_g I(M_4-M_3)\ ,\\
\dot{M}_3 &= -\gamma_R M_3+\gamma'_R M_1+2\mathcal{B}_g I(M_4-M_3)\ ,\\
\dot{M}_2 &= -(R_{21}+R_{20}+\mathfrak{P})M_2-\mathfrak{P}M_1+\gamma_R M_4\\
&\quad -\gamma'_R M_2+\mathfrak{P}N_{CO_2}\ ,\\
\dot{M}_1 &= -R_{11'}M_1+R_{21}M_2+\gamma_R M_3-\gamma'_R M_1\ ,\\
\dot{M}_{1'} &= R_{11'}M_1-R_{1'0}M_{1'}\ ,\\
\dot{M}_0 &= -\mathfrak{P}M_0+R_{1'0}M_{1'}\ .
\end{aligned} \tag{B3}$$

Using the same procedure applied above to derive the memory function, we find

$$\mathcal{H}^*=\frac{2\gamma_R/\gamma'_R}{\dfrac{1}{\gamma'_R}+\dfrac{R_{11}\left[1+\dfrac{\mathfrak{P}}{R_{1'0}}\right]-R_{20}}{R_{11'}(R_{21}+R_{20}+\mathfrak{P}\left[1+\dfrac{R_{21}}{R_{1'0}}\right]+\mathfrak{P}R_{21}}}\ . \tag{B4}$$

For the operating conditions of our discharge an adiabatic elimination of the $M_3$ and $M_4$ variables may be applied so that only the $M_1$ and $M_2$ variables will be used. By adopting the model of Fig. 1(a) with the amplifier's populations normalized to $N_{CO_2}$, the number of molecules per unit volume of the amplifier, the equations ruling $D=(M_2-M_1)/N_{CO_2}$ and $S=(M_2+M_1)/N_{CO_2}$ become

$$\dot{D}=-\left[\frac{R_{20}+R_{10}}{2}+R_{21}+4B_g I\right]D-\left[\frac{R_{20}-R_{10}}{2}+R_{21}+\mathfrak{P}\right]S+\mathfrak{P}\ , \tag{B5a}$$

$$\dot{S}=-\frac{R_{20}-R_{10}}{2}D-\left[\frac{R_{20}+R_{10}}{2}+\mathfrak{P}\right]S+\mathfrak{P}\ , \tag{B5b}$$

where the sum $B_g$ has been defined,

$$B_g=\mathcal{B}_g\gamma'_R/\gamma_R\ , \tag{B5c}$$

as a result of the adiabatic elimination and of the smallness of the transition rate induced by the radiation compared to the one due to relaxation toward the vibrational manifold. To take into account the effect of the population normalization as well of the above approximation we have also defined

$$B_{sg}=\mathcal{B}_{sg}N_{CO_2}\gamma'_R/\gamma_R\ . \tag{B5d}$$

## APPENDIX C: RELAXATION DYNAMICS IN THE ABSORBER

The derivation of the rate equations associated to the absorption mechanism follows that introduced in a previous paper.[2] By referring to Fig. 2 we will denote with $\overline{M_3}$

and $\overline{M_4}$ the population of the resonant lower and upper level and with $\overline{M_1}$ and $\overline{M_2}$ the population in the ground- and excited-state vibrational band excluding the resonant levels. By considering that a vibrational relaxation takes place out of both upper level 2 and lower level 1, measuring times in units of $1/(2k)$, normalizing the relaxation rates to $2k$, and making use of Eq. (6c), we can write

$$\begin{aligned}
\dot{\overline{M_4}} &= -\overline{\gamma_R}\,\overline{M_4} + \overline{\gamma'_R}\,\overline{M_2} - 2\mathcal{B}_a I(\overline{M_4} - \overline{M_3}) , \\
\dot{\overline{M_3}} &= -\overline{\gamma_R}\,\overline{M_3} + \overline{\gamma'_R}\,\overline{M_1} + 2\mathcal{B}_a I(\overline{M_4} - \overline{M_3}) , \\
\dot{\overline{M_2}} &= -\overline{\gamma_v}\,\overline{M_2} + \overline{\gamma_R}\,\overline{M_4} - \overline{\gamma'_R}\,\overline{M_2} , \\
\dot{\overline{M_1}} &= -\overline{\gamma_V}\,\overline{M_1} + \overline{\gamma_R}\,\overline{M_3} - \overline{\gamma'_R}\,\overline{M_1} .
\end{aligned} \tag{C1}$$

If we introduce the variables $\delta_R = (\overline{M_3} - \overline{M_4})/N_a$ and $\Delta_v = (\overline{M_1} - \overline{M_2})/N_a$, respectively, for the population differences between the resonant levels and the vibrational bands of the absorber, with $N_a$ the number of absorber molecules per unit volume and in the velocity range interacting with the field, this set of equations can be transformed into the following:

$$\dot{\delta}_R = -\overline{\gamma_R}\,\delta_R + \overline{\gamma'_R}\,\Delta_v - 2\mathcal{B}_a \delta_R I , \tag{C2a}$$

$$\dot{\Delta}_V = -\overline{\gamma_v}(\Delta_v - \Delta_v^0) + \overline{\gamma_R}\,\delta_R - \overline{\gamma'_R}\,\Delta_v . \tag{C2b}$$

In Eqs. (C2a) and (C2b) $\delta_R^0$ and $\Delta_R^0$ represent the thermal equilibrium values for the rotational and vibrational population difference. In order to conform to the notation used in Eq. (9) for the amplifier medium we have defined the symbols

$$B_a = \mathcal{B}_a , \tag{C2c}$$

$$B_{sa} = \mathcal{B}_{sa} N_a . \tag{C2d}$$

---

*Present address: Laboratoire de Spectroscopie Hertzienne, Université de Lille I, 59655 Villeneuve d'Ascq CEDEX, France.

[1]N. B. Abraham, P. Mandel, and L. M. Narducci, in *Progress in Optics*, edited by E. Wolf (North-Holland, Amsterdam, 1988), Vol. XXV, pp. 1–190. In conformity to this review we will refer to the traditional terminology of mean-field approximation as uniform-field approximation.

[2]E. Arimondo, F. Casagrande, L. Lugiato, and P. Glorieux, Appl. Phys. B **30**, 57 (1983).

[3]T. Erneux and P. Mandel, Z. Phys. B **44**, 353 (1981); Phys. Rev. A **30**, 1902 (1984); P. Mandel and T. Erneux, *ibid.* **30**, 1893 (1984).

[4]E. Arimondo, in *Instabilities and Chaos in Quantum Optics II*, edited by N. B. Abraham, F. T. Arecchi, and L. Lugiato (Plenum, New York, 1988), pp. 69–82.

[5]M. Tachikawa, K. Tanii, M. Kajita, and T. Shimizu, Appl. Phys. B **39**, 83 (1986).

[6]J. Tulip, IEEE J. Quant. Electron. **QE-6**, 206 (1970).

[7](a) C. Dang, J. Reid, and B. K. Garside, Appl. Phys. B **27**, 145 (1982); (b) C. Dang, J. Reid, and B. K. Garside, Appl. Phys. B **31**, 163 (1983); (c) C. Dang, J. Reid, and B. K. Garside, IEEE J. Quantum Electron. **QE-19**, 755 (1983).

[8]F. DeTomasi, D. Hennequin, B. Zambon, and E. Arimondo, J. Opt. Soc. Am. B **6**, 45 (1989).

[9](a)R. Salomaa and S. Stenholm, Phys. Rev. A **8**, 2695 (1973); **8**, 2711 (1974); (b) Appl. Phys. **14**, 355 (1977).

[10]D. E. Chyba, N. B. Abraham, and A. M. Albano, Phys. Rev. A **35**, 2936 (1987).

[11]See, for instance, M. Sargent, M. O. Scully, and W. Lamb, Jr., *Laser Physics* (Addison-Wesley, Reading, MA, 1974).

[12]See F. T. Arecchi and R. G. Harrison, *Instabilities and Chaos in Quantum Optics* (Springer-Verlag, Berlin, 1987).

[13](a) O. R. Wood II, P. L. Gordon, and S. E Schwarz, IEEE J. Quantum Electron. **QE-5**, 502 (1969); (b) I. Burak, P. L. Houston, D. G. Hutton, and J. I. Steinfeld, IEEE J. Quantum Electron. **QE-7**, 73 (1971).

[14](a) M. Tachikawa, K. Tanii, and T. Shimizu, J. Opt. Soc. Am. B **4**, 387 (1987); (b) K. Tanii, M. Tachikawa, M. Kajita, and T. Shimizu, J. Opt. Soc. Am. B **5**, 24 (1988); (c) M. Tachikawa, M. Tanii, and T. Shimizu, J. Opt. Soc. Am. B **5**, 1077 (1988); (d) M. Tachikawa, F. L. Hong, M. Tanii, and T. Shimizu, Phys. Rev. Lett. **60**, 2266 (1988).

[15]D. Hennequin, F. DeTomasi, B. Zambon, and E. Arimondo, Phys. Rev. A **37**, 2243 (1988).

[16]K. Fox, Opt. Commun. **19**, 397 (1976); C. Salomon, Thèse de Docteur de 3ème cycle, Université de Paris–Nord, 1979; C. Bréant, Thèse de Docteur es Sciences, Université de Paris–Nord, 1985.

[17]M. L. Asquini and F. Casagrande, Nuovo Cimento D **2**, 917 (1983).

[18]E. Arimondo and B. M. Dinelli, Opt. Commun. **44**, 277 (1983); E. Arimondo, B. M. Dinelli, and E. Menchi, in *Optical Bistability II*, edited by C. K. Bowden, H. M. Gibbs, and S. L. McCall (Plenum, New York, 1984), pp. 317–324.

[19]E. Arimondo, D. Dangoisse, C. Gabbanini, E. Menchi, and F. Papoff, J. Opt. Soc. Am. B **4**, 892 (1987).

[20]E. Arimondo and E. Menchi, Appl. Phys. B **37**, 55 (1985).

[21]J. J. Degnan, Appl. Phys. **11**, 1 (1976).

[22]P. F. Moulton, D. M. Larsen, J. M. Walpole, and A. Mooradian, Opt. Lett. **1**, 51 (1977).

[23]A. V. Devir and U. P. Oppenheim, Appl. Opt. **8**, 2121 (1969).

[24]R. S. McDowell, H. W. Galbraith, C. D. Cantrell, N. G. Nereson, P. F. Moulton, and E. D. Hinkley, Opt. Lett. **2**, 97 (1978).

[25]E. H. M. Hogenboom, W. Klische, C. O. Weiss, and A. Godone, Phys. Rev. Lett. **55**, 2571 (1985); W. Klische and C. O. Weiss, Phys. Rev. A **31**, 4049 (1985).

[26]B. Comaskey, R. E. Scotti, and R. L. Shoemaker, Opt. Lett. **6**, 45 (1981).

[27]U. P. Oppenheim and Y. J. Kaufmann, IEEE J. Quantum Electron. **QE-10**, 533 (1974).

[28]D. E. Chyba, J. Phys. (Paris) C **2**, 367 (1988); D. E. Chyba and N. B. Abraham (unpublished).

[29]H. Brunet, IEEE J. Quantum Electron. **QE-6**, 678 (1970).